PHOTOMASK

BACUS—The international technical group of SPIE dedicated to the advancement of photomask technology.

Actinic EUVL mask blank inspection capability with time delay integration mode

Takeshi Yamane, Toshihiko Tanaka, Tsuneo Terasawa, and Osamu Suga,
MIRAI-Semiconductor Leading Edge Technologies (Selete) Inc., 16-1 Onogawa, Tsukuba-shi, Ibaraki 305-8569, Japan

ABSTRACT

We have been developing an actinic full-field mask blank inspection system to detect multilayer phase defects with dark field imaging. Using the current system, we have analyzed the probability of defect detection and occurrence of false defects with variations in defect signal intensity and in background intensity. The result indicates that the size of the smallest defect for 100% detection with no false defect at full-field inspection is 2.0 nm in height and 78 nm in width. A 100% detection of smaller defects, 1.5 nm high and 60 nm wide, with no false defect at full-field inspection requires 46% reduction of the detection threshold. This means that for further improvement of defect sensitivity, a 46% reduction of CCD noise level, or improvement of the defect detection algorithm, will be required.

1. Introduction

Extreme Ultraviolet lithography (EUVL) is a promising technology for ULSI devices with a half pitch of 32 nm and below. However, the fabrication of defect-free mask blanks and their inspection continue to be a matter of concern for the implementation of EUVL. A multilayer phase defect is initiated by some kind of disorder in the multilayer that is generated during the multilayer film growth if a particle or a pit happens to reside on a quartz substrate surface. Because this kind of defect is hardly noticeable on the mask blank surface with a conventional inspection system, an actinic (at wavelength) defect inspection technique is being pursued.[1-10]

Continues on page 3.

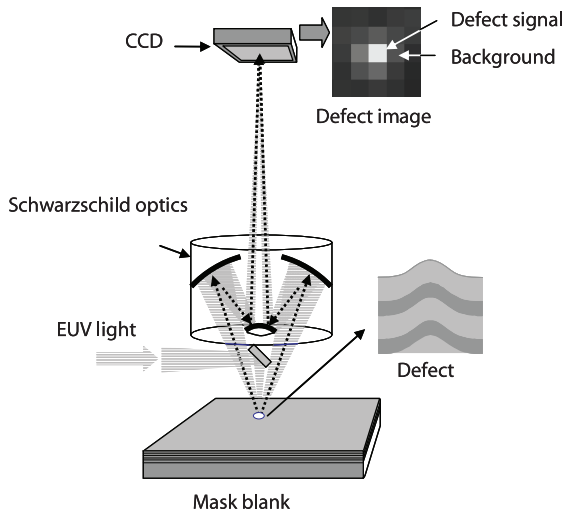

Figure 1. Actinic inspection of multilayer mask blank with dark-field imaging.

BACUS NEWS

November 2009
Volume 25, Issue 11

SPIE

EDITORIAL

A New Market for Mask Makers: Patterned Media

Douglas J. Resnick, Molecular Imprints

The twin forces of consumer demand and innovative new technologies are remaking the hard disk drive industry and—in the process—creating a significant new market for mask makers. The ever-growing demand for hard drives with greater storage density is driving a technology shift from continuous magnetic media to patterned media hard disks, which are expected to be implemented in hard disk drives to provide data storage at densities exceeding 1012 bits per square inch. Realization of this technology transition will require industrial-scale lithography at unprecedented levels of feature resolution, pattern precision, and cost efficiency. This technology was highlighted in September, during four sessions at the 29th Annual Photomask Technology Conference.

Two primary approaches for patterned media have been proposed to overcome the limits associated with superparamagnetism. In the simplest example, lithography and etch processes are employed to isolate each bit of data in a precise island of magnetic material. Each bit is patterned individually, so this approach is termed "bit-patterned media" (BPM). The lithographic entry point from a resolution standpoint, is a pitch of 50nm, quickly dropping from 25nm. Practical implementation requires a number of rapid advances in template fabrication, etching of magnetic material, addressing of the drive head element, etc. The challenges of the BPM approach to patterned media are being addressed by an intermediate approach, in which individual tracks of data are patterned instead of individual bits. This approach is termed "discrete track recording" (DTR) and the patterns comprise dense arrays of lines.

It is anticipated that the double sided media will be patterned using ultra-violet nanoimprint lithography which will require an imprint mask or "template". Conventional electron-beam write tools that might be used to define the patterns on a template have x-y stages and operate by stitching together adjacent exposure fields. But patterned media applications have very low tolerance for the stitching errors that inevitably occur at the boundaries between exposure fields. Fabrication of the template will require electron-beam writing systems with a rotating stage. This configuration is well-suited for defining the concentric layouts that are required for patterned media applications, and several suppliers now offer such systems. These systems will produce a single master template in 1-2 weeks, resulting in very high cost. Therefore, this template will be used as a master which will be replicated using imprint lithography on tools specifically designed for this purpose. These replication tools can produce over ten templates an hour, making the replicas a fraction of the master cost.

In addition to maintaining the critical dimension defined on the master, new techniques will be needed to qualify the replica. While the defect levels are substantially relaxed relative to semiconductor requirements, it is clear that pattern inspection will occur at multiple points during the lithography process, beginning with the qualification

Continued to page 6.

BACUS N • E • W • S

BACUS News is published monthly by SPIE for BACUS, the international technical group of SPIE dedicated to the advancement of photomask technology. Circulation 2600.

Managing Editor/Graphics Linda DeLano
Advertising Teresa Roles-Meier
BACUS Technical Group Manager Pat Wight

SPIE

P.O. Box 10, Bellingham, WA 98227-0010 USA
Tel: +1 360 676 3290 or +1 888 504 8171
Fax: +1 360 647 1445
SPIE.org
customerservice@spie.org

Continued from cover.

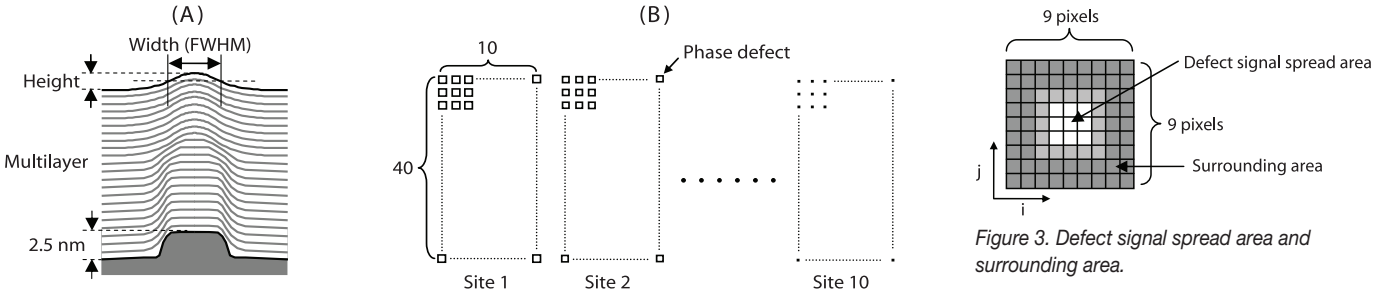

Figure 2. (A) Structure and (B) layout of programmed phase defects.

Figure 3. Defect signal spread area and surrounding area.

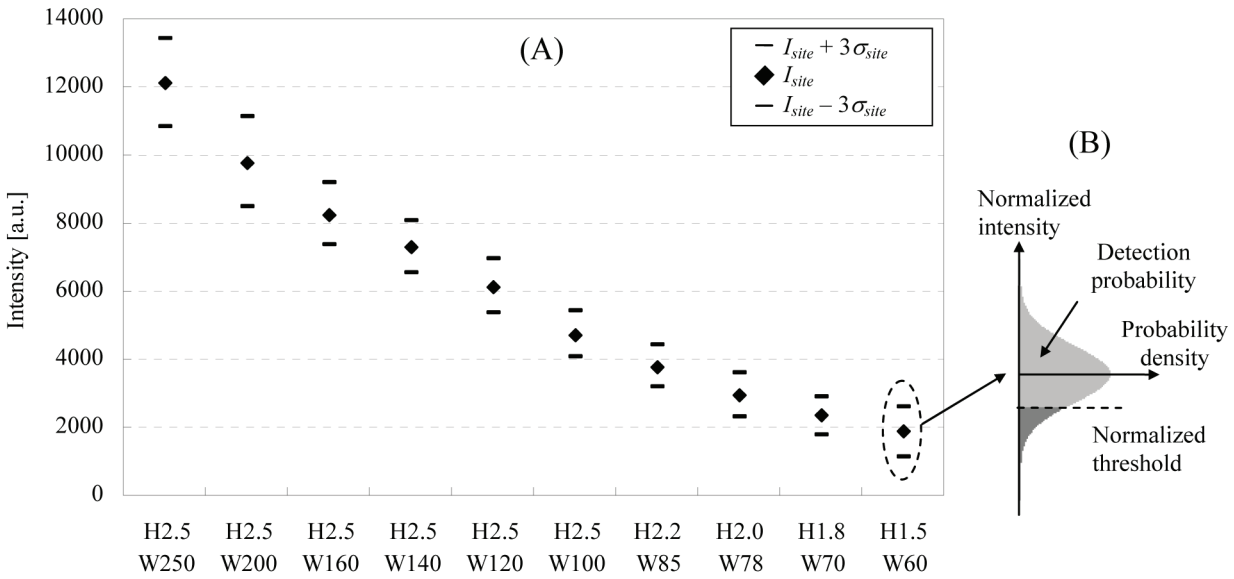

Figure 4. (A) Variation of defect signal intensity with defect dimension measured by AFM. (B) Detection probability on Gaussian distribution with threshold normalized by I_{site} and σ_{site}.

To address this issue, we have developed an actinic full-field EUVL mask blank inspection system to detect multilayer phase defects by employing a dark field imaging technique. Based on our estimation of impact of a phase defect on a wafer for 22 and 32 nm HP devices, we set our target of inspection sensitivity to be capable of capturing a phase defect caused by a 1.5 nm-high and 40 nm-wide protrusion on a multilayer surface. Such a system has been fabricated, and after its final tune-up and optimization of its full-field inspection capability, the system has now become available.

In this system, the light scattered from a mask blank surface propagating in a direction between the inner and outer NAs of a Schwarzschild optics reaches a CCD camera where a defect is captured as a spot signal brighter than the background intensity of the surrounding area. The stage of the system scans the full field of a mask blank to capture images with time delay integration (TDI) method. With the obtained images, the system can detect a defect as a spot signal brighter than a pre-determined threshold. Variation in defect signal intensity is caused primarily due to variation of illumination intensity. If a threshold is set at a level lower than that of the defect signal intensity, the defect will be detected with almost 100% probability, even if the defect signal intensity fluctuates. On the other hand, background intensity varies primarily due to CCD noise. If the threshold is set at a level much higher than that of the background intensity, any variation of background intensity would not be registered as a false defect, and therefore, any occurrence of a false defect will be almost zero. However, high probability of defect detection and low occurrence of a false defect turn out to be two goals in conflict. The occurrence of a false defect increases in proportion to the increase in the inspection area. Therefore, in order to minimize a false defect at full-field inspection area, defect sensitivity will have to be sacrificed.

For this work, the probability of defect detection and the occurrence of the false defects were analyzed with variations of defect signal intensity and of background intensity. Variation of defect signal intensity was evaluated with programmed phase

Continues on page 4.

Continued from page 3.

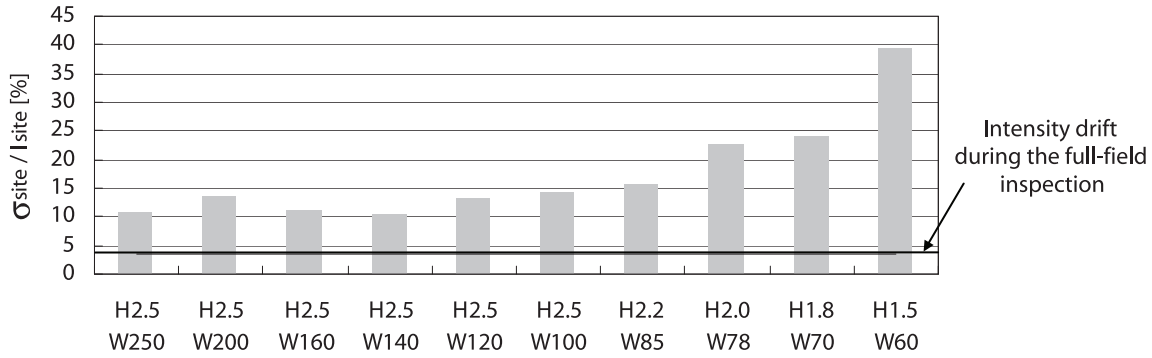

Figure 5. The ratio of σ_{site} to I_{site} with intensity drift during the full-field inspection.

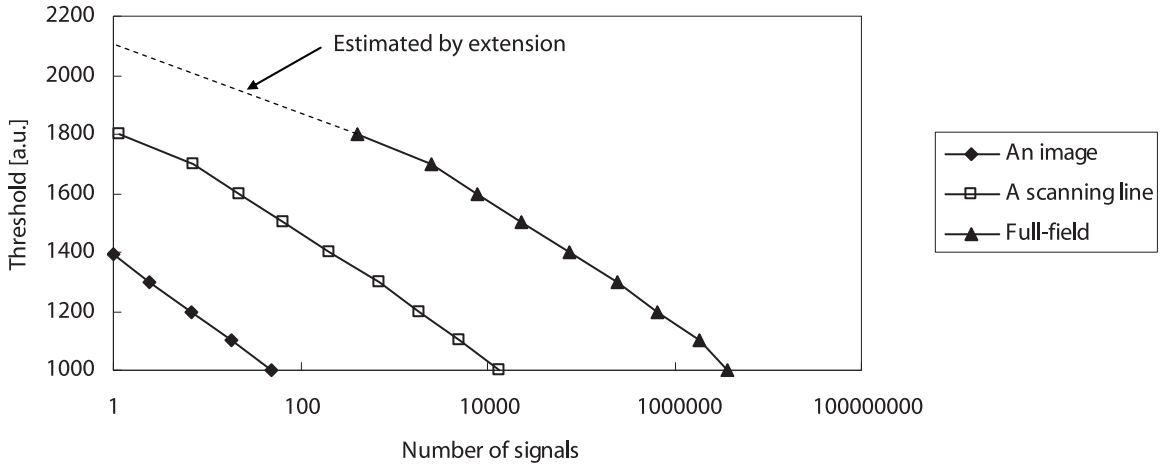

Figure 6. Number of signals larger than threshold at an image, a scanning line, and full-field areas.

defects on a mask blank, whereas variation of background intensity was evaluated with a mask blank. And then, defect detection probability with no false defect was estimated. Furthermore, target of the CCD noise reduction for the improvement of defect sensitivity with no false defect was also determined.

2. Configuration of the acting inspection system

The actinic full-field inspection system is based on an experimental study on MIRAI II project. The system consists of EUV light source, illumination optics containing ellipsoidal and plane mirrors, Schwarzschild optics for dark field imaging, and EUV-sensitive backside-illuminated CCD camera.[3-5] As described in Fig. 1, EUV light collected and polarized for 90 degrees on an ellipsoidal mirror (not shown) is reflected by a plane mirror (located under the convex mirror of the Schwarzschild optics) and illuminates a mask blank. The scattered light from the mask blank propagating in the direction between the inner and outer NAs of the Schwarzschild optics reaches the CCD camera, while the reflected light from the mask blank is shielded. The inner NA is fixed to 0.1, while the outer NA varies from 0.20 to 0.27. In this work, the outer NA of 0.2 was used. The pixel size of the CCD used was 500 nm at the object plane. In this set up when a defect happens to be on the mask blank, the incident light is scattered by it and then captured as a spot signal brighter than signals at the surrounding pixels viewed as the background intensity.

3. Variation of defect signal

The variation of defect signal intensity was evaluated with programmed defects on a mask blank. The programmed defects were produced by 2.5 nm-high dots formed on the quartz substrate. These dots created protrusions in the multilayer which then formed bump phase defects (Fig. 2). The defects were arranged in a matrix of 10 x 40 arrays at 10 different sites, where the target dimensions of the dots varied with sites. The height and full width at the half maximum (FWHM) of the protrusions on the multilayer surface (Fig. 2), were measured by an atomic force microscope (AFM).

The programmed defects were captured during the scanning at a speed of 1 mm/s using TDI method. Defect signal was characterized by its peak against a background intensity

BACUS N • E • W • S

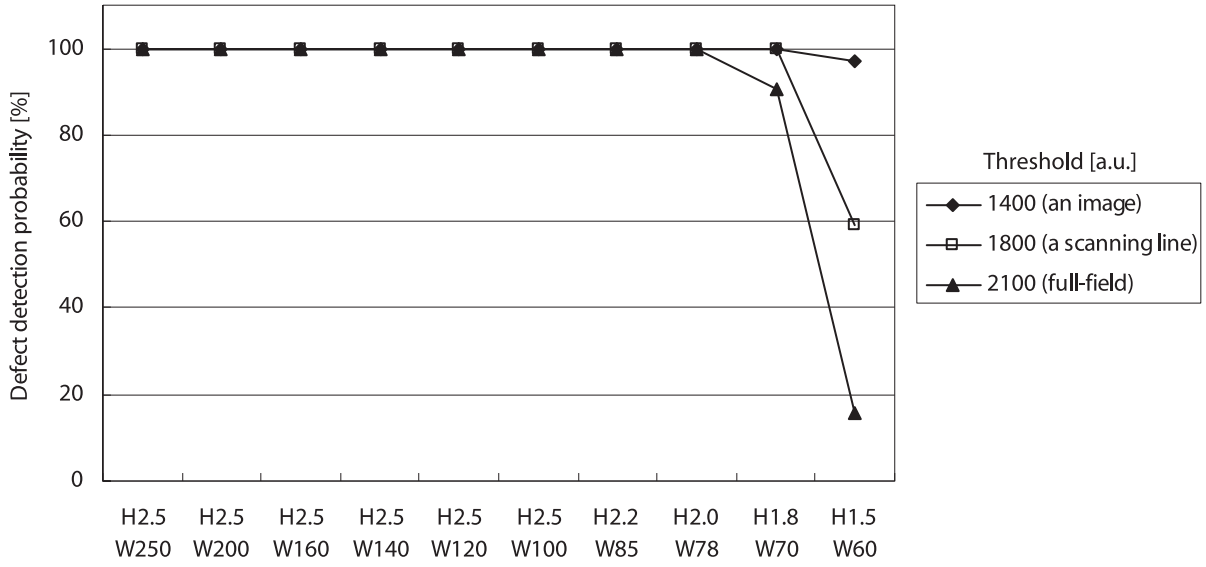

Figure 7. Defect detection probability with the thresholds for no false defect at an image, a scanning line, and full-filed areas.

generated by mask blank surface roughness, and where due to the electron diffusion in CCD, the region of the signal was spread over 3x3 pixels. Hence, the defect signal intensity (S_{defect}) was calculated as:

$$S_{defect} = \sum_{3x3\ pixels} (I_{ij} - BGL) \quad (1)$$

I_{ij} means signal intensity of a pixel located on (i, j), *BGL* means averaged intensity at the surrounding area represented by 56 pixels, and summation range of 3x3 pixels means the defect signal spread area (Fig.3). The defects were captured 5 times and from which, standard deviations (σ_{defect}) of S_{defect} on each of the defects were calculated. Variation of defect signal intensities (σ_{site}) was calculated as pooled σ_{defect} of 20 defects on each site. The averaged defect signal intensity (I_{site}) was obtained as an average of S_{defect} of 20 defects on each site. Figure 4 shows I_{site} with variation range of $+/-3\sigma_{site}$ and defect dimensions measured by AFM.

Figure 5 shows the ratio of σ_{site} to I_{site} with intensity drift during a full-field inspection of 14 hours and 15 minutes. These ratios are found to be larger than the intensity drift. Especially, the ratio of the smallest defect, 1.5 nm high and 60 nm wide, indicates 39.3%, and is much larger than the intensity drift of 3.4%.

4. Occurrence of false defect

The variation of background intensity was evaluated using a mask blank. A mask blank with no programmed defects was inspected by scanning with a velocity of 1mm/s. The area of the scanning line was 140 mm x 0.5 mm. The signal intensities of the captured images were calculated using the same procedure as in the case of S_{defect} using equation (1). The signals of real defects were eliminated from those of the captured images by reviewing the found defects. In the rest of the signals, the signals, whose intensities were larger than a threshold, were counted as shown in Fig. 6. Numbers of signals at an image area, 0.5 mm square, were calculated as the numbers at a scanning line area multiplied by the area ratio of 1/280. In the same way, numbers at full-field area of 140 mm square were calculated as the numbers at a scanning line area multiplied by the area ratio of 280. The dotted line shown in Fig. 6 was estimated by an extension of the signal numbers at full-field area. As shown in Fig. 6, thresholds for 1 signal at an image, a scanning line, and fullfield area were found to be 1400, 1800, and 2100 respectively. These thresholds caused 1 or less than 1 false defect at an image, a scanning line, or full-field inspection, and therefore, indicated thresholds for no false defect at the applied areas.

5. Defect detection probability with no false defect

The probability of detecting a defect of each of the 10 defect dimensions with no false defect was estimated. Using the variation of defect signal intensity and the thresholds for no false defect, existing probability of the defect signals larger than the threshold was calculated with Gaussian distribution, illustrated in Fig. 4 (B). The intensity drift during the inspection was neglected for this calculation because the intensity drift was much smaller than the variation, especially for small defects whose signal intensity was close to the threshold. The calculated probabilities are shown in Fig. 7. With the threshold of 1400, causing no false defect at an image area, the probability indicated almost 100% for each of 10 defect dimensions. With the threshold of 2100, causing no false defect at full-field area, the probability for 1.5 nm high 60 nm wide defect indicated 16%. In the case where ($I_{site} - 3\sigma_{site}$) was larger than at the threshold, the probability was more than 99.86% and assumed to be as 100%. The smallest defect for 100% probability with no false defect at fullfield inspection was 2.0 nm high and 78 nm wide. With the threshold of 1125, the probability on each of the 10 defect dimensions became to be 100%. Hence, 100%

Continues on page 6.

Continued from page 5.

detection for 1.5 nm high and 60 nm wide defect with no false level or defect detection algorithm will be required.

6. Summary

We have developed an actinic full-field EUVL mask blank inspection system. Defect detection probability and false defect occurrence on the inspection system were analyzed. The result indicated that the current inspection capability with no false defect at full-field of a mask blank was found to be 2.0 nm high and 78 nm wide defect detection. To detect 1.5 nm high and 60 nm wide defect at 100% probability with no false defect at full-field, the detection threshold must be reduced by 46%. Therefore, the 46% reduction of a CCD noise level or improvement of defect detection algorithm will be required for further improvement of defect sensitivity.

7. Acknowledgment

The authors are grateful to HOYA Corporation for the programmed defect mask fabrication and AFM measurement. This work was supported by New Energy and Industrial Technology Development Organization (NEDO).

8. References

[1] T. Tomie, T. Terasawa, Y. Tezuka, and M. Ito, "Concept of ultra-fast at-wavelength inspection of defects on multilayer mask blanks using a laser-produced plasma source," *Proc. SPIE* **5038,** 41 (2003).

[2] E. M. Gullikson, E. Tejnil, T. Liang, and A. Stivers, "EUVL Defect Printability at the 32 nm node," *Proc. SPIE* **5374,** 791 (2004).

[3] Y. Tezuka, M. Itoh, T. Terasawa, and T. Tomie, "Actinic Detection and Signal Characterization of Multilayer Defects on EUV Mask Blanks," *Proc. SPIE* **5567,** 791 (2004).

[4] T. Terasawa, Y. Tezuka, M. Itoh, and T. Tomie, "High Speed Actinic EUV Mask Blank Inspection with Dark-Field Imaging," *Proc. SPIE* **5446**, 804 (2004).

[5] Y. Tezuka, M. Itoh, T. Terasawa, and T. Tomie, "Actinic Detection and Screening of Multilayer Defects on EUV Mask Blanks using Dark-field Imaging," *Proc. SPIE* **5446,** 870 (2004).

[6] T. Tomie, "Method and apparatus for inspecting multilayer masks for defects," United States Patent 6,954,266 (2005).

[7] Y. Tezuka, T. Tanaka, T. Terasawa, and T. Tomie, "Sensitivity-Limiting factors of at-Wavelength Extreme Ultraviolet Lithography mask Blank Inspection," *Jpn. J. Appl. Phys.* **45(6B),** 5359 (2006).

[8] T. Tanaka, Y. Tezuka, T. Terasawa, and T. Tomie, "Detection signal analysis of actinic inspection of EUV mask blanks using dark-field imaging," *Proc. SPIE* **6152,** 61523U (2006).

[9] K. A. Goldberg, A. Barty, Y. Liu, P. Kearny, Y. Tezuka, T. Terasawa, J. S. Taylor, H. S. Han, and O. R. Wood, "Actinic inspection of extreme ultraviolet programmed multilayer defects and cross-comparison measurements," *J. Vac. Sci. Technol.* **B 24(6),** 2824 (2006).

[10] T. Yamane, T. Iwasaki, T. Tanaka, T. Terasawa, O. Suga, and T. Tomie, "Actinic EUVL mask blank inspection and phase defect characterization," *Proc. SPIE* **7379,** 73790H (2009) *Proc. of SPIE* **Vol. 7488,** 74881B-6.

EDITORIAL *(continued from page 2.)*

A New Market for Mask Makers: Patterned Media

of master templates. Again, the preferred technology is optical inspection on a tool equipped with a rotating stage. These tools were originally developed for monitoring Angstrom-level variations in the thickness of lubrication layers and have since been used for measuring surface roughness, micro-scratches, and particles with sub-100nm sensitivity.

Now, let's look at the market opportunity. Today, the projected lifetime of an imprint template is approximately 10,000 imprints, consequently an original master template could be replicated 10,000 times. These replica templates would then be capable of printing one hundred million disks on one side, 50 million on both sides. When patterned media enters production, approximately a billion disks will need to be patterned, which will require 200,000 replica templates. It will also require many masters to accommodate the various media fabs, disk sizes, and design changes. This is an excellent business opportunity for a mask companies and the vendors that provide the supporting infrastructure!

In summary, despite the challenges, patterned media is a train that's leaving the station which will bring extended life to the HDD areal density roadmap, racing to and beyond a 1TB/in2 threshold. Those players that board early will reap the rewards.

Industry Briefs

SPIE/BACUS: Patterned media is fertile ground

By **Franklin Kalk,** Toppan Photomask

Magnetic disks are exploring new ways to pack more magnetic islands onto 2.5/3.5-in. platters. Today's media, comprised of planar magnetic films deposited on Al or glass, pack 300Gb in a square inch. The roadmap at terabit/in^2 densities requires new architectures as the islands that constitute the bits of information become less stable as their dimensions shrink. One option requires patterning the surface i.e., uses lithography and metrology. Patterned media come as discrete (grooved surfaces) and bit-patterned (individually defined magnetic dots). Nanoimprint requires a master relief pattern to be written in resist and transferred into silicon or quartz, replicated on up to 10 million disks from a single master fabricated on 6-in. silicon or fused silica. The wafer is first coated with an electron-sensitive resist and exposed on a rotary stage Gaussian spot electron-beam writing system, typically with 100 keV voltage, followed by developing and dry etching. DNP described the system with track pitches as low as 44nm, Hoya's discrete track media uses 2.5-in. quartz masters with track pitches down to 50nm. By adjusting chain volume, degree of polymerization and mixture ratio, two immiscible polymers can be mixed to form regular structures such as arrays of spheres, lamellae, or cylinders of one material in another.

Media mastering is much different that making a conventional IC photomask. The writing takes 10-20 days and a 100% master pattern inspection with an electron beam tool, more than one day. Mastering costs will be high unless the equipment can find other uses while a pattern is being written. SEM CD measures quartz nanoimprint templates—first optimizing the beam for quartz feature metrology, then using simulation to extract profile information without cross-sectioning. X-ray scatterometry is required to measure pitch to within 0.1nm and to reconstruct the fine details of feature profiles on magnetic substrates, including corner rounding, wall angle, CD and height. In summary, this year's BACUS points the way to patterned media as an expanding topic with fertile development ground.

New Reticle Inspection System

By **Mark LaPedus,** EE Times

KLA-Tencor Corp. has rolled out its new reticle defect inspection system. Targeted for the 2x-nm logic (3x-nm half-pitch memory) node, the new Teron 600 platform brings programmable scanner-illumination, computational lithography and other capabilities. The system, which has inspected prototype reticles created for inverse lithography technology, source-mask optimization, double-patterning lithography and EUV, is engineered to be extendible to potential 1x-nm optical solutions.

The Teron 600 features a new, 193-nm wavelength light source to improve image processing for high-resolution reticle plane inspection (RPI). It provides die-to-database and die-to-die operating modes, supports wafer-plane inspection (WPI) for prediction of reticle defect printability, complete with photoresist thresholding and modeling of sub-wavelength diffraction and polarization effects. It also includes a user-configurable scanner illumination model, enabling prediction of reticle defect printability.

According to KLA, the dramatic change in reticle strategy for the 2x-nm device generation has created a discontinuity in reticle defect inspection. The reticle features are much smaller than one would predict from a 3x-nm to 2x-nm shrink. In addition, the mask pattern is so fractured that it is no longer feasible for an engineer to look at the location of a reticle defect and decide whether it is likely to print on the wafer—and potentially cause a catastrophic yield loss. For the 2x-nm node, one must be able to input a custom scanner illumination profile, take into account polarization effects and the photoresist, and rigorously calculate the impact of the reticle defect on the wafer.

Join the premier professional organization for mask makers and mask users!

About the BACUS Group

Founded in 1980 by a group of chrome blank users wanting a single voice to interact with suppliers, BACUS has grown to become the largest and most widely known forum for the exchange of technical information of interest to photomask and reticle makers. BACUS joined SPIE in January of 1991 to expand the exchange of information with mask makers around the world.

The group sponsors an informative monthly meeting and newsletter, BACUS News. The BACUS annual Photomask Technology Symposium covers photomask technology, photomask processes, lithography, materials and resists, phase shift masks, inspection and repair, metrology, and quality and manufacturing management.

Individual Membership Benefits include:

- Subscription to BACUS News (monthly)
- Complimentary Subscription *Semiconductor International* magazine
- Eligibility to hold office on BACUS Steering Committee

spie.org/bacushome

Corporate Membership Benefits include:

- One Voting Member in the SPIE General Membership
- Subscription to BACUS News (monthly)
- One online SPIE Journal Subscription
- Listed as a Corporate Member in the BACUS Monthly Newsletter

spie.org/bacushome

Calendar

2009

SPIE Lithography Asia - Taiwan

18-19 November
Sheraton Taipei Hotel
Taipei, Taiwan
spie.org/la

2010

SPIE Advanced Lithography

21-26 February
San Jose Marriott and
San Jose Convention Center
San Jose, California, USA
spie.org/al

Late abstracts will be considered by the Chairs.

SPIE Photomask Technology

13-17 September
Monterey Marriott and
Monterey Conference Center
Monterey, California, USA
spie.org/pm

Abstract submissions will open in late November.

You are invited to submit events of interest for this calendar. Please send to lindad@spie.org; alternatively, email or fax to SPIE.

SPIE is an international society advancing light-based technologies.

SPIE
International Headquarters
P.O. Box 10, Bellingham, WA 98227-0010 USA
Tel: +1 888 504 8171 or +1 360 676 3290
Fax: +1 360 647 1445
customerservice@spie.org • SPIE.org

Shipping Address
1000 20th St., Bellingham, WA 98225-6705 USA

SPIE Europe
2 Alexandra Gate, Ffordd Pengam, Cardiff,
CF24 2SA, UK
Tel: +44 29 20 89 4747
Fax: +44 29 20 89 4750
spieeurope@spieeurope.org • www.spieeurope.org